Rapid Analysis of Platinum and Nafion Loadings Using Laser Induced Breakdown Spectroscopy

Yun Wang,[a,*,z] Jianlong Yu,[b] Jingtian Wu,[a] and Zhe Wang[b,z]

[a]*Renewable Energy Resources Lab, Department of Mechanical and Aerospace Engineering, The University of California, Irvine, Irvine, California 92697-3975, USA*
[b]*State Key Lab of Power Systems, Department of Thermal Engineering, Tsinghua University, Beijing 100084, People's Republic of China*

Pt and Nafion are materials widely used in electrochemical devices including PEM fuel cells, flow batteries, electrolyzers, and electrochemical sensors. In PEM fuel cells, the catalyst layer consists of multiple materials including catalyst Platinum (Pt) or Pt-based alloys, carbon, and ionomer (usually Nafion). Laser induced breakdown spectroscopy (LIBS) is a promising analytical tool for probing the elemental composition in a sample, offering advantages of fast, in-situ, and online analysis, minimal sample preparation requirement, and the capability of spontaneous multi-element analysis. In this paper, we present a study of probing the Pt and Nafion loadings in their mixtures with graphite carbon, respectively, using LIBS technology. Pt-carbon and Nafion-carbon samples of various material loading are prepared for the LIBS testing. Plasma plume and shadowgraphic images are presented to show plasma and associated shockwave evolution. It takes a few milliseconds for spectrum collection per laser shot. Each sample analysis contains 49 shots in the present study and takes less than 1 minute. The results show LIBS is capable of probing the Pt and Nafion loadings in the mixtures. The method is useful in rapid analysis of catalyst layer composition and examination of material loss due to degradation.

Due to the growing concerns on the depletion of petroleum-based energy resources and climate change, PEM fuel cells have received much attention in recent years owing to their high efficiencies and low emissions.[1–4] PEM fuel cells are electrochemical devices that directly convert chemical energy stored in fuels such as hydrogen to electrical energy with an efficiency as high as 60% in electrical energy conversion and overall 80% in co-generation of electrical and thermal energies.[5] Among various components, the catalyst layer (CL), where the hydrogen oxidation reaction (HOR) or oxygen reduction reaction (ORR) takes place, is one of the most important and complex parts in PEM fuel cells.[6]

Several phases contained in a CL are key to the electrochemical reaction: 1) carbon support with Pt particles dispersed on the carbon surface, 2) ionomer, and 3) void space, see Fig. 1. The catalyst plays the critical role of reducing the reaction activation barrier for the electrochemical reactions and its loading determines electrode electrochemical performance. Platinum or platinum alloy is popular catalyst for both the ORR and HOR, therefore the CL contributes a significant portion of cost for a PEM fuel cell. The DOE target is 0.125 mg PGM/cm^2 by 2020, and the 3M Company achieves 0.13 mg PGM/cm^2 in 2015.[7,8] Ionomer is the transport network for protons. Its content, tortuosity, and water content in a CL determine the proton (or ionic) resistance, which can be significant under dry operation. Wang and Feng[9] showed that the ionic resistance in a CL could be a limiting factor, leading to local reaction variation. They defined a dimensionless parameter ($\bar{h} = \frac{\Delta U}{2\frac{R_g T}{\alpha_c F}}$ where $\Delta U = \frac{I\delta}{\sigma_m^{eff}} = IR_\delta$) based on the ionic resistance to quantify the spatial variation of local reaction rate.

LIBS, a type of atomic emission spectroscopy, has been considered as a "future superstar" in analytical chemistry field, with the advantages of fast, in-situ, and online analysis, minimal sample preparation requirement and the capability of spontaneous multi-element analysis.[10–13] It employs a highly energetic laser pulse as the excitation source to atomize and excite samples with plasma formation. The characteristic radiation is collected when the species in the plasma decayed from a higher energy level to lower energy level, and sent to the spectrometer and detected by a CCD or ICCD camera. The spectra contain information of the chemical composition in the sample, which can be used for both qualitative and quantitative purposes. LIBS has been applied to many areas such as metallurgy, environmental monitoring, space exploration and geology. Specially, some studies

explored quantification of Pt group elements[14–16] using LIBS. Multi-layered materials were also investigated using LIBS.[17–19] In addition, several other types of spectral analysis techniques are available for chemical composition detection, including Raman spectroscopy, inductively coupled plasma atomic emission spectroscopy (ICP-AES), and X-ray fluorescence (XRF). Raman spectroscopy is a method that observes vibrational, rotational, and other low-frequency modes in a system to identify molecules and study chemical bonding. ICP-AES uses the inductively coupled plasma to produce excited atoms and ions that emit electromagnetic radiation at characteristic wavelengths and detects elements in the sample. XRF is the emission of characteristic fluorescence from a material that is excited by high-energy X-ray and is widely used for elemental and chemical analysis.

To date, few studies were proposed to analyze the CL composition information, providing that the CL composition is a preset parameter in CL fabrication. It is however possible that the CL physical properties change due to phase change or aggregation during fabrication or due to degradation including loss of ionomer/carbon support and Pt migration.[20] In addition, Wang and coworkers[21,22] proposed multi-layer configuration of CLs, in which the CL contains a few sublayers of specified material composition. It will be valuable to know the material composition in each sublayer of a fabricated multi-layer CL. In this study, we applied the LIBS method to probe the Pt and Nafion loadings in their mixtures with carbon. We used graphite powders as the carbon source to mix with Platinum and Nafion in the sample preparation. Samples of various Pt-carbon and Nafion-carbon ratio were fabricated for testing. Plasma plume, shadowgraphic, and crater images were presented to show physical phenomena occurring during LIBS testing. Linear relationships were shown for both cases, indicative of potential applicability of LIBS to analyze the loadings of important materials in fuel cell electrodes.

Catalyst Layer in PEM Fuel Cell

Fig. 1 schematically shows a fuel cell structure and electrode catalyst layers (CLs). The CLs are the thin layers (∼10 μm) coated on the membrane surface, containing catalyst (typically Platinum), carbon, ionomer electrolyte, and void space. Nano particles of catalyst platinum attach on the surface of supporting carbon powders with electrolyte ionomer covering on the surfaces, forming the triple-phase boundaries (TPBs). In the anode/cathode, the HRR/ORR takes place at the TPBs:
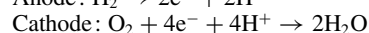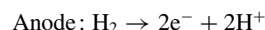
$$\text{Anode}: H_2 \rightarrow 2e^- + 2H^+$$
$$\text{Cathode}: O_2 + 4e^- + 4H^+ \rightarrow 2H_2O \qquad [1]$$

*Electrochemical Society Member.
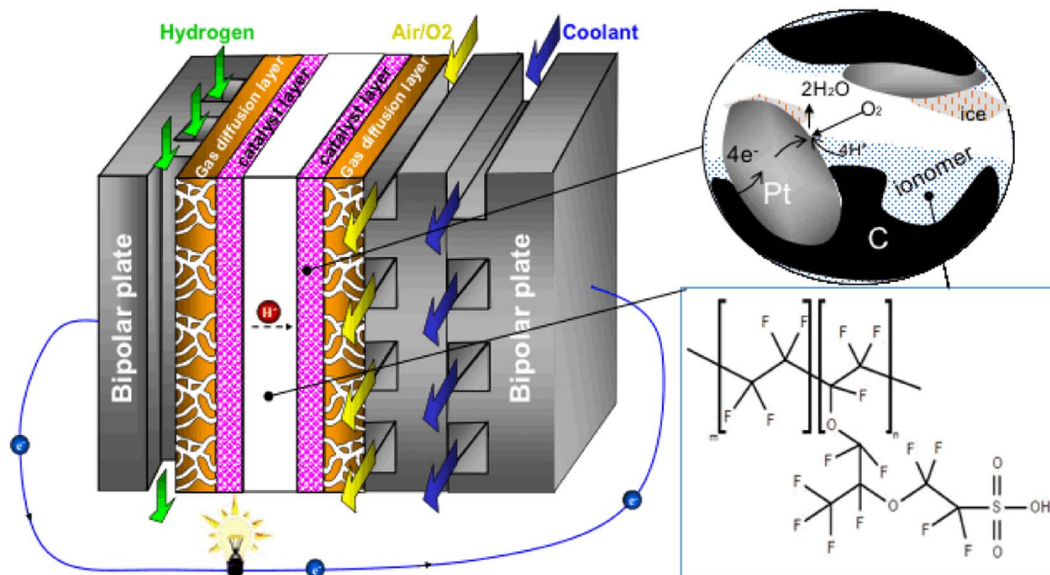[z]E-mail: yunw@uci.edu; zhewang@tsinghua.edu.cn

Figure 1. Schematic of a PEM fuel cell and structures of the catalyst layer and electrolyte ionomer Nafion.

The constituent materials in CLs provide transport paths for reactants. For example, carbon powders are the media for electron transport while protons travel through the ionomer electrolyte phase. Water and heat are produced as the only byproducts. Water is transported in both electrolyte and void phases. The Pt and ionomer loadings are important for the catalyst layer function. The catalyst loading determines the active surface area and contributes a major portion of a fuel cell cost.[5,6] In CLs, the catalyst nanoparticles reside on the carbon support in order to be electrochemically active. The common Pt loading in commercial CLs ranges from 0.1–0.4 mg/cm^2. The ionomer network in CLs conducts protons for the electrochemical reactions and is a key parameter limiting the local reaction rate.[9] Fig. 2 presents three fabricated catalyst layers under various configuration, showing that the CLs are usually thin, around 10 μm. The CL composition, both Pt loading and ionomer (*I*) content, significantly influences fuel cell performance, as shown in Fig. 3. The current ionomers are mostly based on the perfluorosulfonic acid, the most prominent of which, Nafion, was first developed by the DuPont Company in 1960 s. Nafion has a backbone structure of polytetrafluoroethylene (PTFE, known by the trade name Teflon), see Fig. 1. The sulfonic acid functional groups in Nafion provide charge sites for proton transport. Additionally, other perfluorinated polymer materials such as Neosepta-F (Tokuyama),

Gore-Select (W.L. Gore and Associates, Inc.), Flemion (Asahi Glass Compnay), Asiplex (Asahi Chemical Industry) are also adopted for PEM fuel cell.[5] For Nafion, the backbone consists of long chains of -(CF2)- and short chains of the function group (-HSO$_3$), see Fig. 1. Given the fixed ratio of F to C in the chain -(CF2)-, the Florine (F) content can be used to evaluate the Nafion loading in the CL. It is difficult to use the carbon (C) element to quantify the Nafion loading because the catalyst carbon support provides another carbon source in CLs.

Experimental

Sample preparation.—In the LIBS testing, Pt-carbon and Nafion-carbon samples of various loading were prepared. The graphite powers were chosen as the carbon source to mix with Platimun and Nafion solutions, respectively.

In the preparation of Nafion-carbon samples, the original Nafion solution of a 10% mass concentration was used and further diluted with deionized water to a concentration of 5% and 2.5%, respectively. A 0.5 ml volume of the new Nafion solution and a certain amount of graphite powers were mixed and then thoroughly stirred in a sample Aluminum box. The mixture was dried for 24 hours before the
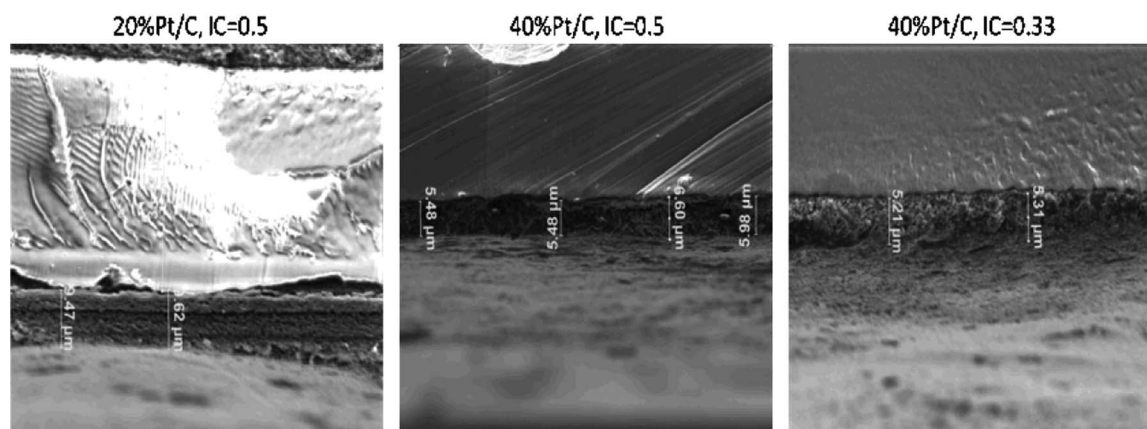

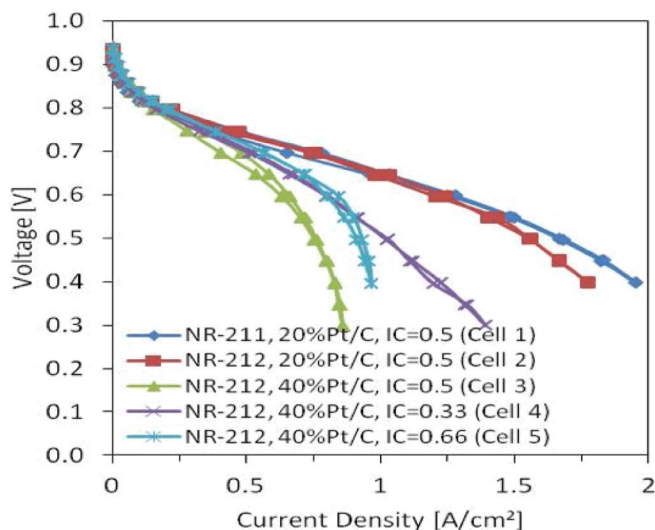**Figure 2.** SEM of the catalyst layer under various Pt, carbon (C) and ionomer (I) loadings.[35]

Figure 3. PEM fuel cell performance under various Pt, carbon, and ionomer loadings for operation of 80°C and 100 %RH.[35]

Table I. Nafion-carbon samples and their specifics.

	Nafion solution	Mass of Nafion/g	Mass of graphite powers/g	Nafion Mass Fraction (IC Ratio)/%
N1	0.5 ml, 10%	0.05	0	100.0
N2	0.5 ml, 10%	0.05	0.03	62.5
N3	0.5 ml, 10%	0.05	0.05	50.0
N4	0.5 ml, 10%	0.05	0.1	33.3
N5	0.5 ml, 10%	0.05	0.2	20.0
N6	0.5 ml, 5%	0.025	0.2	11.0
N7	0.5 ml, 2.5%	0.0125	0.2	5.9

Nafion-carbon samples were used for LIBS. Figure 4 presents the fabricated Nafion-carbon and pure Nafion samples for testing. The graphite powers in the sample are bonded by the Nafion ionomer. Totally seven Nafion-carbon samples were prepared for LIBS testing with their configuration given in Table I.

For the Pt-carbon samples, a commercial Pt solution of 1 mg Pt/mL in the hydrochloric solvent was used. A certain volume of the Pt solution was taken and mixed with 0.1 g graphite powers, followed by 24 hours drying. Figure 4 presents the image of a Pt-carbon mixture sample. Each testing sample is 4 cm^2 in size, thus the lowest Pt loading (the P1 case in Table II) is corresponding to 0.05 mg Pt/cm^2. Totally, six samples of various Pt loading were prepared for LIBS testing with their configuration listed in Table II.

LIBS measurement.—The samples were tested using a LIBS experimental system, an integrated LIBS device (ChemReveal) manufactured by TSI (Minnesota, USA), see Fig. 5. A pulsed laser at 1,064 nm was emitted and focused on the sample surface by a convex lens.
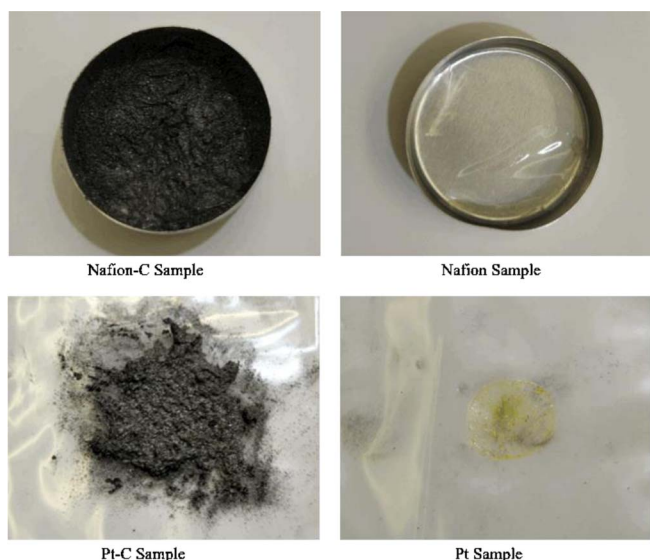
The duration of laser was 5 ns and the pulse energy was adjusted to 105 mJ for an appropriate signal intensity. The optical emission of induced plasma was collected by a fiber system and delivered to a spectrometer that ranges approximately from 180–1000 nm. A CCD camera was placed to record the optical signal. The delay time between the laser occurrence and the CCD detection was set 1 us and the gate width was 1 ms. Totally 49 (7 × 7) shots were taken for each sample to get the average emission intensity to decrease the influence of random fluctuation in experiment.

The laser-induced plasma images were captured by an integrated LIBS system (Applied Spectra, USA). We employed a Q-switched Nd:YAG laser (Quantel, France) with a wavelength of 1,064 nm, a pulse width of 8 ns, and a spot size of around 60 μm in diameter. The plasma plume images were captured by an ICCD camera (Andor, UK) under different ICCD settings, including the gate widths, gains, pre-amplifier gains and optical filter types, to obtain the images with optimal image quality at different delay times. The shockwave images were captured separately using another integrated LIBS system (Applied Spectra, USA) with the plasma produced using a Q-switched Nd:YAG laser (Beamtech, China) with a wavelength of 1,064 nm and pulse width of 8 ns. Another Q-switched Nd:YAG laser (Quantel, France) with a 532 nm wavelength and 500 ps pulse width serves as the probe laser providing the light source to the shadowgraph formation.

Results and Discussion

Fig. 6 (above) shows plasma formation and expansion, along with shockwave propagation, during the LIBS testing. In the testing, the high-power laser added a large amount of heat to a small spot area in a very short time, leading to evaporation of local sample material and further formation of plasma. Typical plasma temperatures of 10,000 K or higher were observed in the early plasma lifetime.[23,24] The high-temperature plasma consists of elements in the sample and environmental gas species, thus its emitted light spectrum carries information of the sample material. The plasma plume last a few milliseconds, in which the LIBS recorded the intensity of emitted light for element analysis. Thus the spectrum collection took a duration of a few milliseconds for each shot. In each sample analysis, total 49 shots were

Nafion-C Sample   Nafion Sample

Pt-C Sample   Pt Sample

Figure 4. Nafion and Nafion-carbon samples (above) and Pt and Pt-carbon samples (below).

Table II. Pt-carbon samples and their specifics.

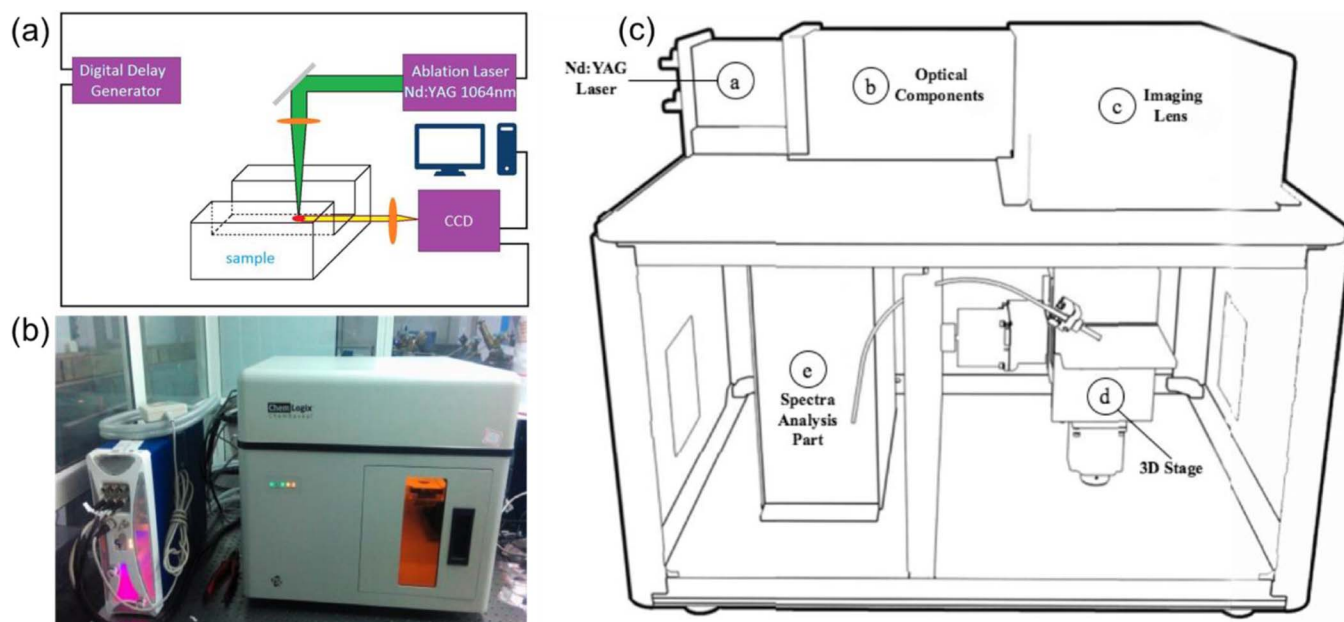|	Pt solution	Mass of Pt/mg	Mass of graphite powers/g	Pt content/ mg/g	Pt loading*/ mg/cm^2
P1	0.2 ml, 1 mg/ml	0.2	0.1049	1.9	0.05
P2	0.3 ml, 1 mg/ml	0.3	0.1048	2.9	0.075
P3	0.4 ml, 1 mg/ml	0.4	0.1046	3.8	0.1
P4	0.5 ml, 1 mg/ml	0.5	0.1045	4.8	0.125
P5	0.7 ml, 1 mg/ml	0.7	0.1051	6.7	0.175
P6	0.8 ml, 1 mg/ml	0.8	0.1052	7.6	0.2

*per sample area.

Figure 5. Schematic of LIBS (a), photo of experimental devices (b), and schematic of the testing device (c).

taken at various sample location with each location movement at a speed of 1 Hz, thus analysis for one sample took less than 1 minute in this study. Note that the speed of LIBS analysis can be further improved. Bette and Noll[25] proposed a high-speed LIBS with laser pulse repetition frequencies of up to 1 kHz for scanning microanalysis of macroscopic samples. In addition, the high energy addition and rapid expansion of the high-temperature plasma also lead to formation of shockwaves, as shown in Fig. 6 (below). In the early stage, the shockwave (e.g. 100 ns) exhibit a shape stretched in the laser incidence direction, primarily caused by plasma eruption. In addition, the theory of laser supported detonation wave (LSD wave)[26] indicates that the energy from the trailing laser pulse increases the temperature and electron density at the shockwave tip, contributing to the non-uniform heating of the shockwave and the observed stretched shape.[27] After the laser energy vanished, the shockwave exhibit a more hemi-spherical shape with a radius R that can be estimated by the classic Taylor-Sedov theory:[28] $R = \xi(\frac{E}{\rho})^{1/n+2}t^{2/n+2}$ where t is the delay time from the initiation of laser illumination, ρ the surrounding gas density,

E the energy released during the explosion process, and ξ a constant determined by the specific heat capacity ratio. For spherical shock-waves, n is equal to 3, yielding $R \sim t^{0.4}$. Several computer models have been developed to numerically capture the shockwave propagation. A cavity method was also proposed to constrain the shockwave to increase the plasma emission intensity.[29–32]

The laser that is shot on the sample usually has a dimension ranging from 10 to 100 μm in diameter.[33] The large amount of heat added to the sample vaporizes a small portion of the sample material in a very short time, leading to plasma eruption and shockwave formation. Craters may form as a result of the material loss and shockwave propagation. Fig. 7 shows the crater formation and dimension in the Nafion-C sample after LIBS. It is seen that the craters have a dimension of about 600 μm in diameter with a maximum depth of about 60 μm. Thus, for PEM fuel cell applications the present LIBS method may damage local catalyst layer, which is usually about 10 μm thick (see Fig. 2). As quick estimate, the laser energy of 100 mJ is able to vaporize about 2 microgram of graphite at its evaporation temperature (assuming
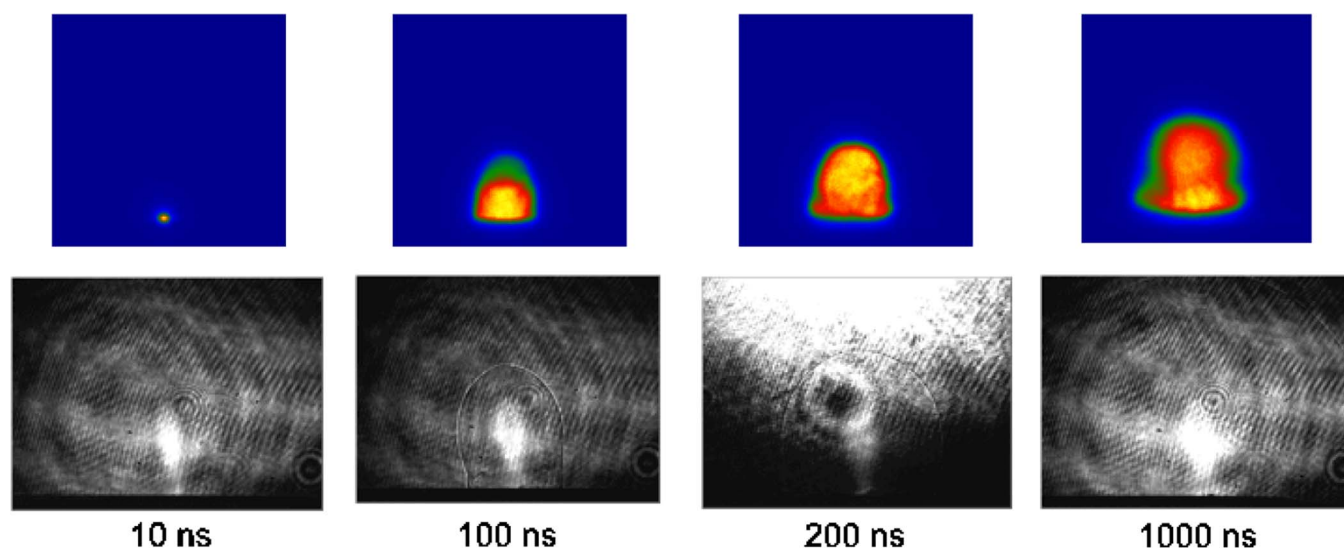

Figure 6. Plasma plume (above) and shadowgraphic (below) images at various time instant.
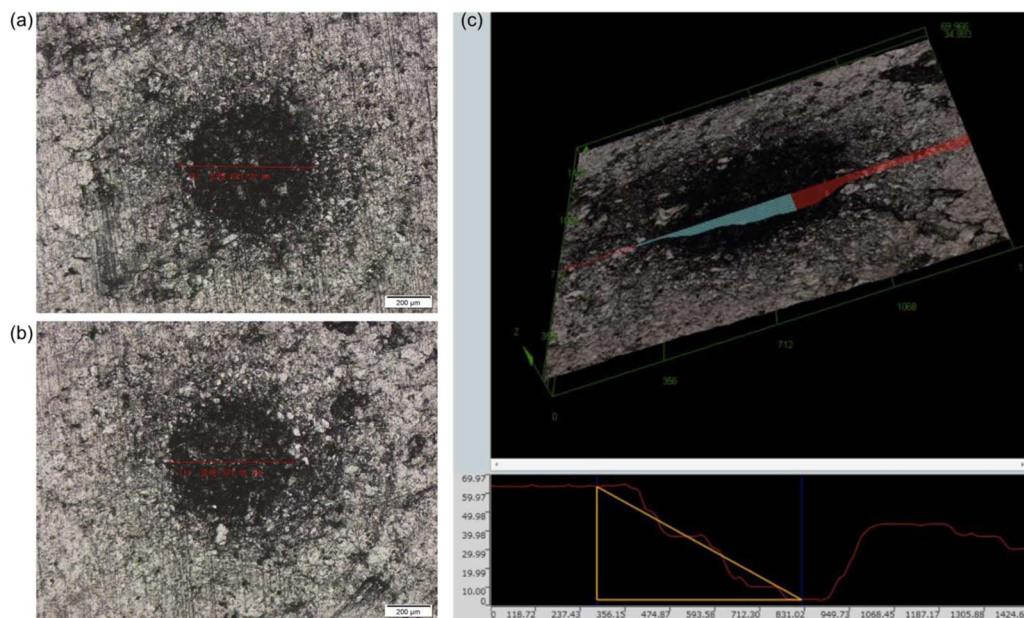
Figure 7. Formation/dimension of craters on the Nafion-carbon sample after LIBS.

the latent heat of evaporation is about 600 kJ/mol under the boiling point of 4,000 K at 1 atm[34]). Note that the above estimate excludes the ionization energy, sensible heat (the plasma temperature reaches ~10,000 K) and latent heat of melting. In addition, the shockwave formation during the LIBS testing causes local high pressure and its fluctuation,[27,32] which may push the surrounding material and enlarge the crater.

Fig. 8 presents the average emission intensity spectrums for the Nafion-carbon (left) and Pt-carbon (right) samples. The spectrums are enlarged near the F line (685.603 nm) and Pt line (306.471 nm), respectively. It shows that different Nafion and Pt loadings yield dif-

ferent emission intensities with a larger loading corresponding to a higher intensity relative to the background one. For N1 (or the pure Nafion case), the spectrum is different with a much lower background intensity due to no carbon presented in the sample.

Fig. 9 presents the emission intensity of the Pt line at 306.471 nm under various Platinum loading. A clear linear relationship was shown for the experimental data, indicative of successful applicability of LIBS in probing Pt loading. Extrapolation of the experimental data falls off the origin point due to the background emission. In addition, a couple of points deviate from the linear line. The observed uncertainty may result from the non-uniform mixing, detector sensitivity, and
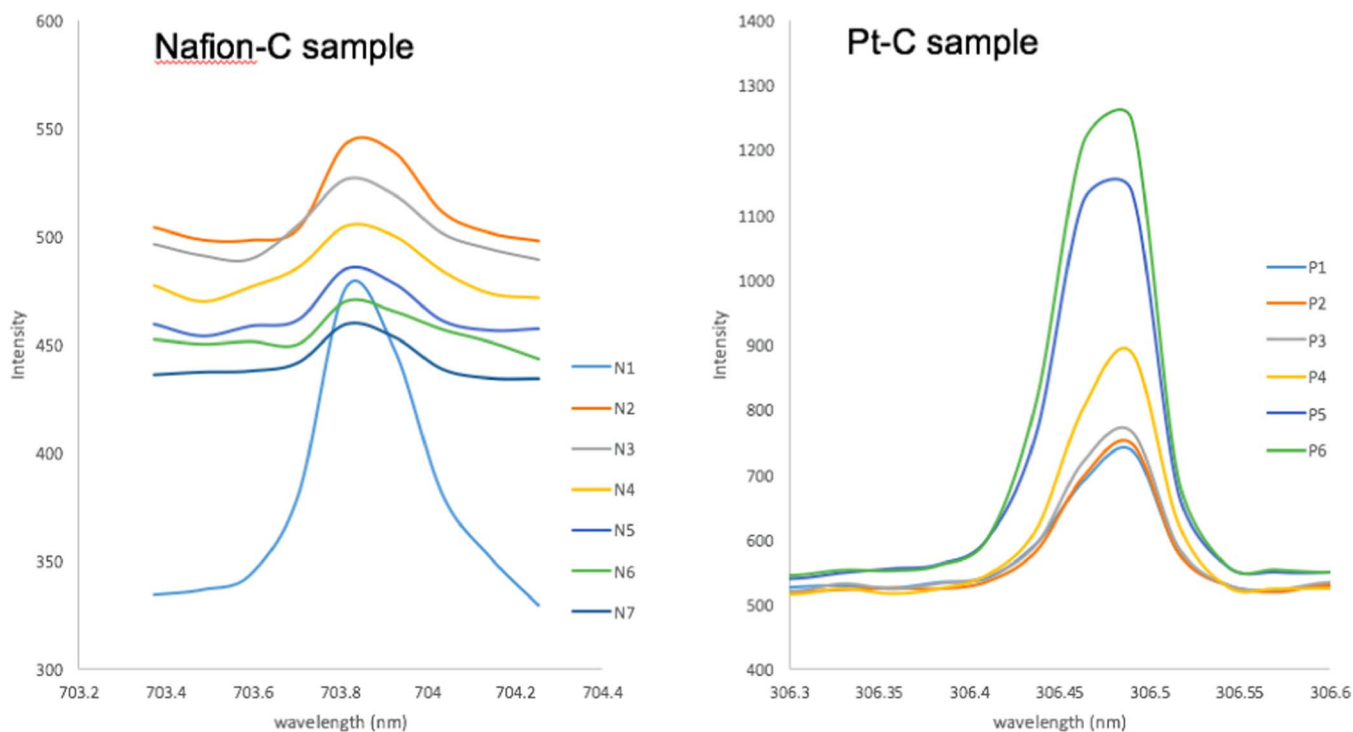

Figure 8. Emission intensity spectrums of the Nafion-carbon and Pt-carbon samples.
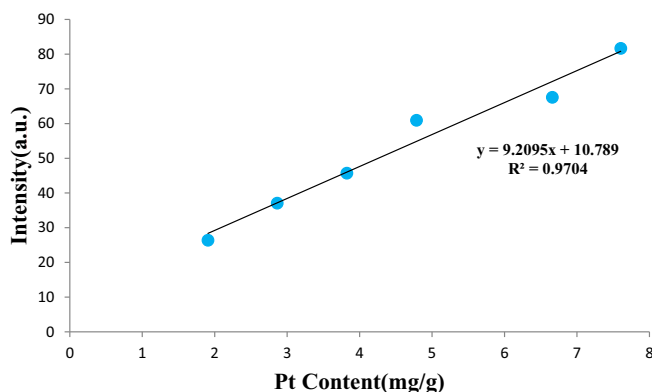
Figure 9. Relationship of Pt emission intensity and Pt loading in Pt-carbon.

plasma morphology fluctuation. Overall, the data points follow the main trend of the linear relationship.

Fig. 10 shows the emission intensity of the F line at 685.603 nm under various Nafion loading, indicating a linear relationship. F is a major constituent in Nafion beside carbon and sulfur. It is difficult to use the element carbon as the working material for spectrum detection because the graphite or carbon support provides another carbon source. In addition, the sulfur (S) emission line in the ultra-violet range will be absorbed by air. Thus, it is difficult to probe the sulfur content in the ambient condition without special treatment. As shown in the figure, selection of the F element in the LIBS testing is successful for probing the Nafion loading. In order to probe the function group [-HSO$_3$] information, it is necessary to explore the sulfur's intensity in the emission spectrum, which is currently under investigation in the labs.

Conclusions

In this paper, we presented a LIBS method to analyze material composition and loading in the Pt-carbon and Nafion-carbon mixtures. Samples of various material loading were prepared for the LIBS testing. Plasma plume, shadowgraphic, and crater images were presented to show the plasma/shockwave formation/propagation and crater dimension in the present LIBS. Major findings are listed as below:

- It is shown in the crater images that the laser shot left a crater of about 600 μm in diameter and about 60 μm in the maximum depth on the sample. Analysis indicated that the laser energy addition is able to vaporize about 2 mg graphite carbon.
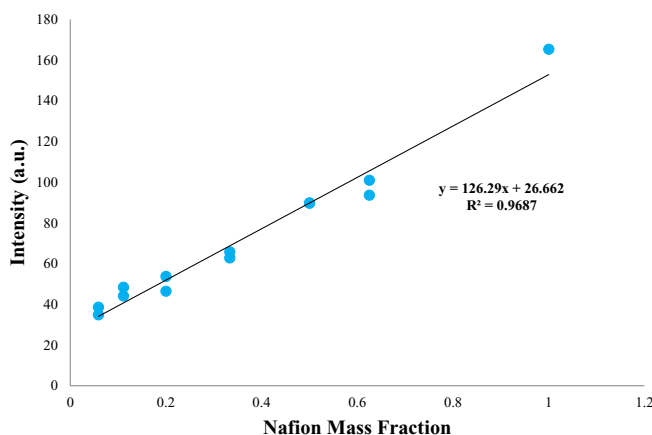

Figure 10. Relationship of F emission intensity and Nafion loading in Nafion-carbon samples.

- Plasma plume and shadowgraphic images showed the laser energy induced formation of high-temperature plasma (for spectrum collection) and shockwave at a time scale of millisecond. The LIBS analysis of one sample required 49 shots/spectrum collections and took less than 1 minute in the present study.
- A linear relationship was indicated between the intensity of Pt spectrum and loading. The LIBS method successfully detected Pt loading at the level of 0.05–0.2 mg/cm^2.
- A linear relationship was indicated between the intensity of F spectrum and Nafion loading. Using the element F, LIBS is capable of probing the Nafion loading in the samples and successfully detected Nafion-carbon ratio ranging from 5.9%–100%.

The LIBS method showed promise in studying material composition in PEM fuel cells and material aging phenomena. Future work includes testing of commercial CL samples, probing other elements in fuel cells, and CL material degradation using LIBS methods.

References

1. James Larminie, Andrew Dicks, and S Maurice, *McDonald. Fuel cell systems explained.*, Vol. **2**. Chichester, UK: J. Wiley, 2003.
2. Ryan O'hayre et al. *Fuel cell fundamentals*, John Wiley & Sons, 2016.
3. Matthew M. Mench, *Fuel cell engines*, John Wiley & Sons, 2008.
4. Y. Wang, K. S. Chen, and S. C. Cho, *PEM Fuel Cells: Thermal and Water Management Fundamentals (Sustainable Energy)*, Momentum Press (2013).
5. Y. Wang, K. S. Chen, J. Mishler, S. C. Cho, and X. C. Adroher, "A Review of Polymer Electrolyte Membrane Fuel Cells: Technology, Applications, and Needs on Fundamental Research", *Applied Energy*, **88**, 981 (2011).
6. Jiujun Zhang, ed. *PEM fuel cell electrocatalysts and catalyst layers: fundamentals and applications*, Springer Science & Business Media, 2008.
7. Steinbach (3M), "High-Performance, Durable, Low-Cost Membrane Electrode Assemblies for Transportation Applications," in *2014 Hydrogen Program Annual Merit Review and Peer Evaluation Meeting*. 2014: Washington, DC.
8. https://www.energy.gov/eere/fuelcells/doe-technical-targets-polymer-electrolyte-membrane-fuel-cell-components
9. Y. Wang and X. Feng, "Analysis of Reaction Rates in the Cathode Electrode of Polymer Electrolyte Fuel Cells Part I: Single-Layer Electrodes", *J. Electrochem. Soc.*, **155**(12), B1289 (2008).
10. D. W. Hahn and N. Omenetto, "Laser-induced breakdown spectroscopy (LIBS), part I: review of basic diagnostics and plasma-particle interactions: still-challenging issues within the analytical plasma community," *Appl. Spectrosc.*, **64**, 335A (2010).
11. D. W. Hahn and N. Omenetto, "Laser-induced breakdown spectroscopy (LIBS), part II: review of instrumental and methodological approaches to material analysis and applications to different fields," *Appl. Spectrosc.*, **66**, 347 (2012).
12. Z. Wang, T. -B. Yuan, Z. -Y. Hou, W. -D. Zhou, J. -D. Lu, H. -B. Ding, and X. -Y. Zeng, "Laser-induced breakdown spectroscopy in China," *Front. Phys.*, **9**, 419 (2014).
13. J. Yu and R. Zheng, "Laser-induced plasma and laser-induced breakdown spectroscopy (LIBS) in China: the challenge and the opportunity," *Front. Phys.*, **7**, 647 (2012).
14. M. A. Palacios et al. "Platinum-group elements: quantification in collected exhaust fumes and studies of catalyst surfaces." *Science of the Total Environment*, **257**(1), 1-15 (2000).
15. P. Lucena, J. M. Vadillo, and J. J. Laserna, "Mapping of platinum group metals in automotive exhaust three-way catalysts using laser-induced breakdown spectrometry," *Anal. Chem.*, **71**, 4385 (1999).
16. P. Lucena and J. J. Laserna, "Three-dimensional distribution analysis of platinum, palladium and rhodium in auto catalytic converters using imaging-mode laser-induced breakdown spectrometry," *Spectrochim. Acta, B*, **56**, 177 (2001).
17. Paul R. D. Mason and Arjan J. G. Mank, "Depth-resolved analysis in multi-layered glass and metal materials using laser ablation inductively coupled plasma mass spectrometry (LA-ICP-MS)." *Journal of Analytical Atomic Spectrometry*, **16**(12), 1381 (2001).
18. J. M. Vadillo and J. J. Laserna, "Depth-resolved analysis of multilayered samples by laser-induced breakdown spectrometry," *J. Anal. Atom. Spectrom.*, **12**, 859 (1997).
19. José M. Vadillo and J. Javier Laserna, "Laser-induced plasma spectrometry: truly a surface analytical tool." *Spectrochimica Acta Part B: Atomic Spectroscopy*, **59**(2), 147 (2004).

20. Rod Borup et al. "Scientific aspects of polymer electrolyte fuel cell durability and degradation." *Chemical reviews*, **107**(10), 3904 (2007).
21. Y. Wang and X. Feng, "Analysis of Reaction Rates in the Cathode Electrode of Polymer Electrolyte Fuel Cells Part II: Dual-Layer Electrodes", *J. Electrochem. Soc.*, **156**(3), B403 (2009).
22. X. Feng and Y. Wang, "Multi-Layer Configuration for the Cathode Electrode of Polymer Electrolyte Fuel Cell" *Electrochimica Acta*, **55**, 4579 (2010).
23. A. K. Knight, N. L. Scherbarth, D. A. Cremers, and M. J. Ferris, *Appl. Spectrosc.*, **54**, 331 (2000).
24. D. A. Cremers and L. J. Radziemski, *Laser Spectroscopy and its Applications*, chapter 5 (New York: Marcel Dekker, 1987).
25. H. Bette and R. Noll, "High speed laser-induced breakdown spectrometry for scanning microanalysis." *Journal of Physics D: Applied Physics*, **37**(8), 1281 (2004).
26. L. J. Radziemski and D. A. Cremers, "Laser-induced Plasmas and Applications," (Marcel Dekker, Inc, 1989).
27. S. Harilal, G. Miloshevsky, P. Diwakar, N. LaHaye, and A. Hassanein, "Experimental and computational study of complex shockwave dynamics in laser ablation plumes in argon atmosphere," *Physics of Plasmas (1994-present)*, **19**, 083504 (2012).
28. Y. B. Zel'dovich, *Physics of Shock Waves and High-temperature Hydrodynamic Phenomena*, (Courier Corporation, 2002).
29. A. M. Popov, F. Colao, and R. Fantoni, "Enhancement of LIBS signal by spatially confining the laser-induced plasma," *J Anal Atom Spectrom*, **24**, 602 (2009).
30. X. Shen, J. Sun, H. Ling, and Y. Lu, "Spatial confinement effects in laser-induced breakdown spectroscopy," *Appl Phys Lett*, **91**, 081501 (2007).
31. Z. Y. Hou, Z. Wang, J. M. Liu, W. D. Ni, and Z. Li, "Signal quality improvement using cylindrical confinement for laser induced breakdown spectroscopy," *Opt Express*, **21**, 15974 (2013).
32. Y. Wang, H. Yuan, F. Yang, and Z. Wang, "Experimental and computational investigation of confined laser-induced breakdown spectroscopy." *Spectrochimica Acta Part B: Atomic Spectroscopy*, **126**, 44 (2016).
33. Andrzej W. Miziolek, Vincenzo Palleschi, and Israel Schechter, eds. *Laser induced breakdown spectroscopy*, Cambridge University Press, 2006.
34. Hugh O. Pierson, "*Handbook of Carbon, Graphite, Diamond, and Fullerenes, Processing, Properties and Applications.*," 18 (1993).
35. J. Mishler, Y. Wang, R. Lujan, R. Mukundan, and R. L. Borup, "An Experimental Study of Polymer Electrolyte Fuel Cell Operation at Sub-Freezing Temperatures," *Journal of The Electrochemical Society*, **160** (6) F514 (2013).